MICROSTRUCTURAL EVOLUTION IN UNDERCOOLED Al–8wt%Fe MELTS

J. Valloton[1], A. A. Bogno[1], J. Chen[2], R. Lengsdorf[3], H. Henein[1],
D. M. Herlach[3], U. Dahlborg[4], and M. Calvo-Dahlborg[4]

[1] Chemical and Materials Engineering, University of Alberta, Edmonton, Canada
[2] NINT, NRC, Edmonton, Canada
[3] Institut für Materialphysik im Weltraum, Deutsches Zentrum für Luft- und Raumfahrt, Köln, Germany
[4]GPM, CNRS-UMR 6634, University of Rouen, France

Keywords: Non-equilibrium solidification, electromagnetic levitation, impulse atomization, Al-8Fe, reduced gravity

Abstract

Containerless rapid solidification of hypereutectic Al–8wt%Fe is investigated experimentally using the Impulse Atomization technique (IA), as well as ElectroMagnetic Levitation (EML) under terrestrial and reduced gravity conditions. The samples were analyzed using scanning and transmission electron microscopy, X-ray and neutron diffraction, as well as electron backscattered diffraction. In both EML and IA, the samples experience some undercooling for the solidification of the primary intermetallic phase, which is likely metastable Al_mFe (m = 4.0–4.4). After recalescence, the solidification path then continues with the nucleation and growth of stable $Al_{13}Fe_4$. While $Al_{13}Fe_4$ dominates in EML samples, it becomes minor in favor of Al_mFe in IA droplets. The morphology differences of the primary intermetallics growing under terrestrial and microgravity conditions in EML are clear with acicular morphology for the former and a star-like morphology for the latter. The α–Al has a strong texture in microgravity EML and in IA samples while a weak one is observed on terrestrial EML. This difference is attributed to the weaker fluid flow occurring under reduced gravity conditions and in IA droplets.

Introduction

Al–based alloys are of high importance for aerospace and automotive industry. Al–Fe basis alloys in particular have long been of interest for high temperature applications such as compressor sections of gas turbine engines and low temperature fan [1–2]. Recent research found new Al–Fe alloy competing with titanium up to 573 K in aerospace structure [3–4]. However, by forming intermetallics such as $Al_{13}Fe_4$ (θ phase), iron can be deleterious to the mechanical properties of aluminum alloy. Thus, strategies have to be developed to modify the negative effect of iron. One of them is by using physical processing such as rapid solidification processing (RSP) to increase the solubility of Fe or obtain finer dissemination of Al–Fe precipitates. The presence of non-equilibrium phases produced by RSP allows greater flexibility and control of the final microstructure to combine good high temperature strength with sufficient ductility, high elastic moduli and excellent thermal stability, superior to those obtained by conventional ingot metallurgy and casting techniques. In this study, containerless rapid solidification of

hypereutectic Al–8wt%Fe is investigated experimentally using the Impulse Atomization technique (IA), as well as ElectroMagnetic Levitation (EML) under terrestrial and reduced gravity conditions.

Experimental

Electromagnetic levitation (EML) is a powerful containerless solidification technique for processing of electrically conducting samples such as metals and semiconductors. By avoiding contact with any container walls and operating under high purity environment, heterogeneous nucleation is strongly reduced and a large range of undercoolings can be achieved. In EML, the sample is placed within a conical levitation coil typically consisting of five to seven water-cooled copper windings with one or two counterwindings at its top (Figure 1, left). Eddy currents are induced in the sample by the electromagnetic field generated by the levitation coils. The sample is heated and molten by ohmic losses, whereas the interaction of these eddy currents with the electromagnetic field leads to a displacement force on the sample that is opposite to the gravitational force. The temperature of the sample is monitored continuously with a contactless pyrometer. To cool the sample below its liquidus temperature and induce solidification, a jet of high purity helium is then used. Detailed information on the EML technique can be found in [5].

Impulse atomization (IA) is the other containerless solidification technique used in this study (Figure 1, right). It consists in the transformation of a bulk liquid into a spray of liquid droplets that solidify rapidly during free fall by losing heat to a surrounding gas of choice (N_2, Ar, or He are commonly used). The bulk liquid is produced by heating a material above its melting point and the atomization is achieved by the application of a pressure (impulse) to the melt, to push it through a nozzle plate with one or several orifices of known size and geometry so that a liquid ligament emanates from each orifice and breaks up into droplets. Cooling rate is both a function of droplet size and the gas used to atomize the molten metal. The solidified powders are then collected in a beaker at the bottom of the atomization tower, washed, and sieved into different particle size ranges for analysis. Detailed information on the IA technique can be found in [6].

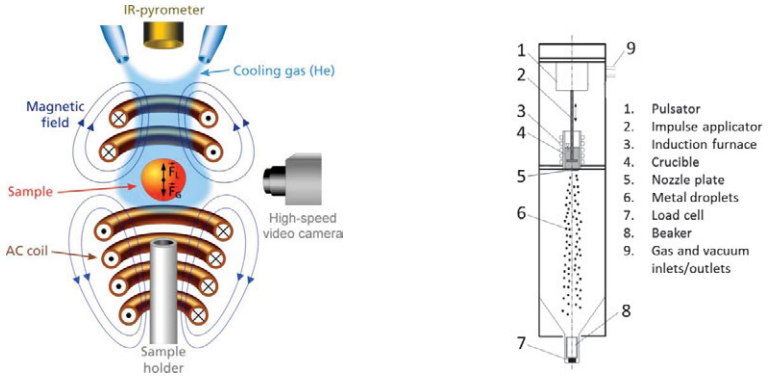

Figure 1. Schematic views of electromagnetic levitation (EML, left) and impulse atomization (IA, right).

Results and Discussion

According to the phase diagram, solidification of Al–8wt%Fe alloy should start with the crystallization of $Al_{13}Fe_4$ intermetallic followed by the eutectic decomposition of the remaining liquid into α–Al and $Al_{13}Fe_4$. Figure 2 shows the microstructure of Al–8wt%Fe EML samples processed under terrestrial (referred as 1g Al–8Fe) and reduced gravity condition (referred as PFC Al–8Fe), (A) and (B) respectively. Temperature measurements show that both samples experienced some undercooling before the solidification of the primary intermetallic phase (ΔT_p = 155 K for 1g and 116 K for PFC) and of the eutectic structure (ΔT_e = 23 K for 1g and 28 K for PFC). The microstructures obtained under those two conditions are different. The primary phase in 1g Al–8Fe is a very acicular-dendritic like morphology, while it has a star-like morphology in PFC Al–8Fe. Some small acicular phase can also be found within the observed area. The existence of star-like morphology suggests PFC Al–8Fe experienced higher cooling rate compared with 1g Al–8Fe. In both samples, α–Al surrounds the primary phase, and the eutectic appears to have formed on the dendrite boundaries between the α–Al matrix.

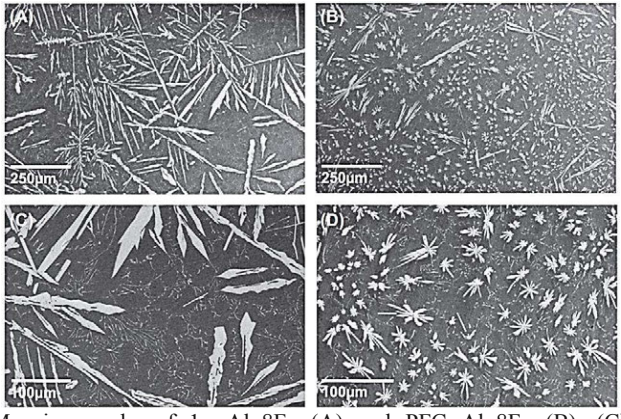

Figure 2. SEM micrographs of 1g Al–8Fe (A) and PFC Al–8Fe (B). (C) and (D) are enlargements of (A) and (B), respectively.

Prior to metallography, neutron diffraction was used for phase identification in the bulk of both samples, together with texture determination. Figure 3 displays the diffraction patterns from 2.6 to 3.2 $Å^{-1}$ (A) and from 1.2 to 2.0 $Å^{-1}$ along with the computed peaks from Rietveld refinement (B). Besides α–Al, the diffraction patterns suggest the existence of $Al_{13}Fe_4$ as well as metastable Al_mFe (m = 4.0–4.4) in the structure for both samples. To corroborate those results, TEM observation was carried out [7]. Selected area electron diffraction pattern simulations (not shown here) confirm unambiguously that the primary intermetallic phase is indeed $Al_{13}Fe_4$ in both 1g and PFC samples. TEM analysis also indicates that the intermetallic within the eutectic is $Al_{13}Fe_4$ as well. Note that in the extensive TEM observation, no Al_mFe was found. However, since the information TEM supplied is from small lamellae taken from the spheres (~6 mm in diameter), it is quite possible that Al_mFe is not in the area investigated. This shows that neutron diffraction and TEM are complementary techniques in the microstructure analysis.

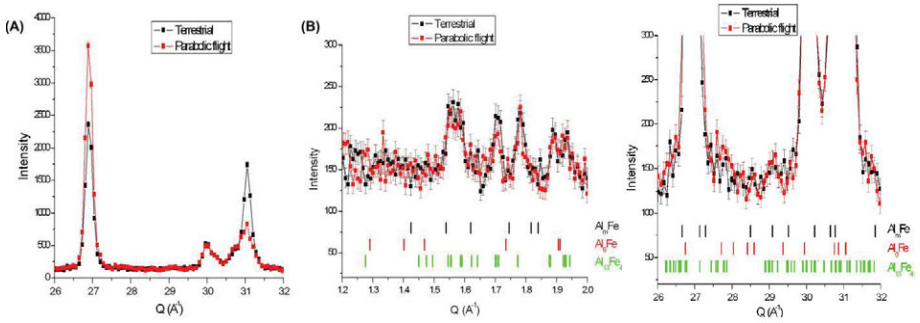

Figure 3. Neutron diffraction spectra of 1g Al–8Fe and PFC Al–8Fe together with Rietveld refinement calculated peaks in (B).

Neutron diffraction also shows a difference in intensity of the α–Al diffraction peaks at about 2.7 and 3.1 Å^{-1} between both samples (Figure 3 (A)). This indicates a difference in texture arising from the difference in solidification of the two samples. However, it seems there are no texture effects neither for Al_mFe nor $Al_{13}Fe_4$; the intermetallic crystals are small and randomly oriented and there is no orientation relationship between α–Al and Al_mFe or $Al_{13}Fe_4$ phases for both samples. Texture of the α–Al phase is also visible on the X-ray diffraction patterns shown in Figure 4 left. The relative intensity of the α–Al peaks in 1g Al–8Fe is almost identical to that of standard JCPDS data, meaning that the microstructure is randomly oriented. On the other hand, the spectrum of PFC Al–8Fe shows an opposite intensity sequence, highlighting a preferred orientation. This is confirmed by electron backscattered diffraction (EBSD, Figure 4 right). From the {110} pole figures it can be seen that the 1g Al–8Fe has a weak texture (C) while texture in sample PFC Al–8Fe is strong (D). This shows the effect of reduced fluid flow in microgravity experiments in this system.

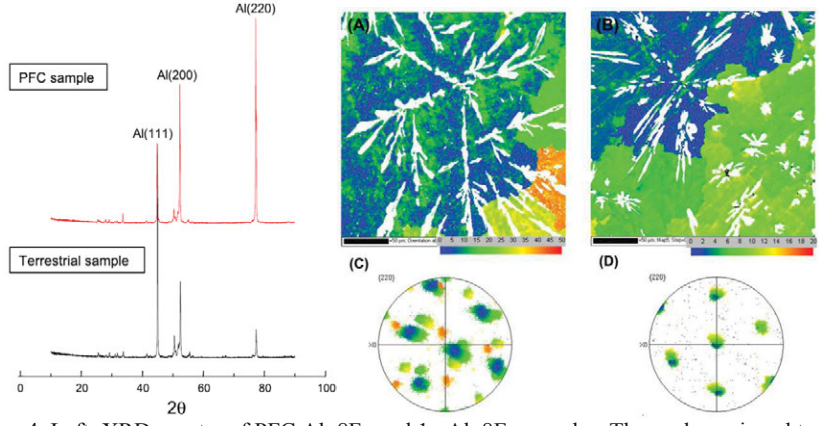

Figure 4. Left: XRD spectra of PFC Al–8Fe and 1g Al–8Fe samples. The peaks assigned to α–Al are marked. The unmarked peaks belong to $Al_{13}Fe_4$. Right: EBSD map of 1 g Al–8Fe (A) and PFC Al–8Fe (B) and their corresponding pole figure ((C) and (D)).

The images shown in Figure 5 are SEM micrographs of a 355 µm Al–8Fe droplet atomized in nitrogen. The microstructure looks somewhat similar to the PFC Al–8Fe sample. The primary intermetallic phase also has a star-like morphology but seems to be blockier. A lamellar α–Al/intermetallic eutectic can also be observed (B), as well as blade-shaped intermetallics in the α–Al matrix (as indicated by arrows in (C)). However, TEM investigation of this sample revealed that the star-shaped primary intermetallic in this case is the metastable Al_mFe, while the blade-shaped intermetallic is the stable $Al_{13}Fe_4$. Furthermore, the simulation of the selected area electron diffraction pattern suggests the intermetallic in the eutectic structure is Al_6Fe. The fact that Al_mFe becomes the major intermetallic phase over $Al_{13}Fe_4$ is confirmed by neutron diffraction (Figure 6). Indeed, the peaks at about 1.42, 1.55, and 1.81 $Å^{-1}$ can be attributed to Al_mFe and are much more pronounced than in the EML samples (Figure 3).

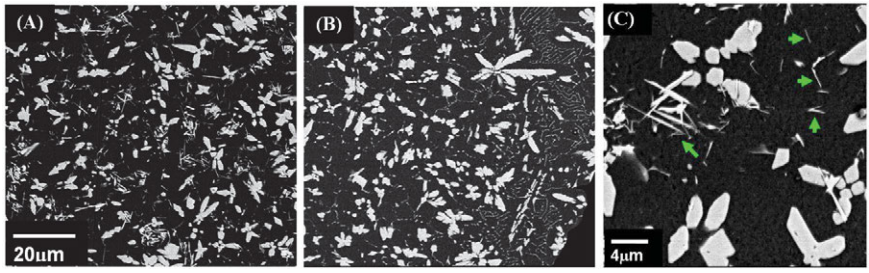

Figure 5. SEM micrographs of a 355 µm Al–8Fe droplet atomized in nitrogen.

According to the aluminum-rich end of the Al-Fe equilibrium phase diagram with metastable extensions, as calculated by Murray [8], we might expect the formation of primary $Al_{13}F_4$, metastable primary Al_6Fe, eutectic α–Al/$Al_{13}Fe_4$, metastable eutectic α–Al/Al_6Fe, or α–Al, depending on the melt undercooling at solidification. Although there is no metastable extension of Al_mFe in Murray's calculation, both differential scanning calorimetry and phase diagram calculation show that Al_mFe has lower metastable eutectic temperature than Al_6Fe [9]. Other research demonstrated that Al_mFe formed at higher cooling rate compared to that of Al_6Fe [10–11]. The existence of primary metastable Al_mFe and stable $Al_{13}Fe_4$ in both 1g and PFC Al–8Fe, as well as in the IA powders, indicates that the primary undercoolings achieved exceed the critical undercooling necessary to form Al_mFe. Otherwise, only stable $Al_{13}Fe_4$ would be present. After nucleation and growth of metastable Al_mFe during recalescence, the rest of the liquid solidifies under quasi-equilibrium conditions with the formation of the stable $Al_{13}Fe_4$ intermetallic. EML samples being much larger than IA droplets, it is expected that for a same undercooling and recalescence event, the proportion of metastable phase in the droplet volume would be larger in IA than in EML. The reason $Al_{13}Fe_4$ dominates the structure in both 1g and PFC Al–8Fe is thus assumed to be the long period of time it has for growth relative to Al_mFe in EML samples. The presence of a metastable α–Al/Al_6Fe eutectic in the IA experiments suggests that the falling droplets either experienced a larger eutectic undercooling than the EML samples or the phase is easier to detect in IA droplets because of the smaller sample volume and higher cooling rate they experience. This higher cooling rate would help retain any metastable structure formed during eutectic nucleation and recalescence.

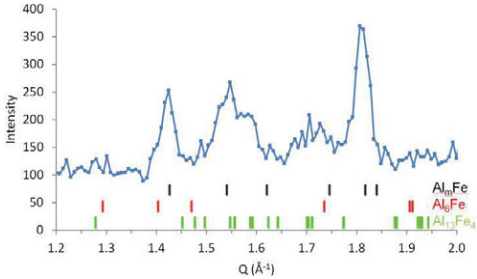

Figure 6. Neutron diffraction spectra of 355 µm Al–8Fe droplets atomized in nitrogen together with Rietveld refinement calculated peaks.

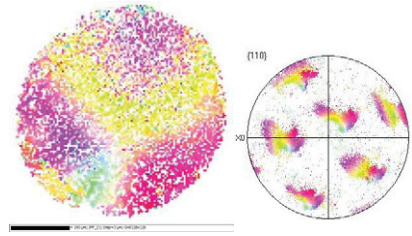

Figure 7. EBSD map and corresponding pole figure of a 355 µm Al–8Fe droplet atomized in nitrogen.

Figure 7 shows the EBSD map and corresponding pole figure of a 355 µm Al–8Fe droplet atomized in nitrogen. Similarly to the the PFC Al–8Fe sample, it can be seen that IA droplets have a strong texture. The pole figure suggests that the α–Al phase in the entire analyzed droplet is made up of one single grain. This again shows the effect of low convection and the similarity of IA experiments to reduced gravity experiments. The smearing of the pole most likely originates from a deformation of the lattice. This can be due to internal stresses occurring during rapid solidification as well as to stresses induced during the mechanical polishing of the sample.

Conclusions

The microstructures of Al–8wt%Fe samples solidified containerless using electromagnetic levitation under different gravity conditions as well as impulse atomization have been studied. The microstructures in EML samples feature primary star-like $Al_{13}Fe_4$ with α–Al/$Al_{13}Fe_4$ eutectic for the droplet experiencing microgravity while the droplet solidified under terrestrial condition is dominated by $Al_{13}Fe_4$ dendrites with α–Al/$Al_{13}Fe_4$ eutectic. Neutron diffraction analysis indicates that, besides the primary $Al_{13}Fe_4$, there is minor metastable Al_mFe (m = 4.0–4.4) in both samples. In the IA droplets, Al_mFe is the major primary intermetallic while $Al_{13}Fe_4$ becomes minor. The eutectic is comprised of α-Al and metastable Al_6Fe, indicating a possibly larger eutectic undercooling than in EML samples. In all cases, metastable Al_mFe is likely the first primary phase to form followed by $Al_{13}Fe_4$ after recalescence. Al_mFe is the dominant intermetallic in the IA droplets due to their small size. $Al_{13}Fe_4$ dominates the structure in both 1g and PFC Al–8Fe because of the long period of time it has for growth relative to Al_mFe in EML samples. This study also demonstrates and contrasts two containerless solidification methods. While it is possible to measure undercooling temperatures in EML, the large sample volume and low cooling rate make it difficult to retain or find the metastable phases in the sample. By contrast with IA, the small droplet sizes and thus their high cooling rate retain the metastable phases formed during undercooling and recalescence. Finally, this study shows that due to their small volume, limited convection occurs in IA droplets during solidification similarly to PFC–EML samples. This is seen in the similar strong texture of α–Al observed in IA and PFC–EML samples but not in the 1g–EML samples.

Acknowledgments

Financial support from the Canadian Space Agency FAST program and the European Space Agency within the NEQUISOL project under contract #4200015236 is acknowledged. Funding form the Natural Sciences and Engineering Research Council of Canada is also acknowledged.

References

[1] D.J. Skinner and K. Okazaki, Rapidly Solidified Powder Aluminum Alloys, ed. M.E. Fine and E.A. Starke Jr (Philadelphia: ASTM, 1986), 211
[2] C.M. Adam, J.W. Simon, and S. Langerbeck, Third Conference on Rapid Solidification Processing: Principles and Technologies, ed. R. Mehrabien (Washington, DC: National Bureau of Standards, 1983), 629
[3] E. Solis-Ramos, H. Jones, and W.M. Rainforth, Mater. Sci. Technol. 22 (2006) 1369
[4] Y. Barbaux and G. Pons, J. Phys. IV 3 (1993), 191
[5] D. M. Herlach, Solidification of Containerless Undercooled Melts, ed. D. M. Herlach and D. M. Matson (Weinheim: Wiley-VCH, 2012), 9–16
[6] H. Henein, Mat. Sci. Eng. A 326 (2002), 92–100
[7] J. Chen, R. Lengsdorf, H. Henein, D. M. Herlach, U. Dahlborg, and M. Calvo-Dahlborg, J. Alloys Compd. 556 (2013), 243–251
[8] J. L. Murray, MRS Symp. Proc. 19 (1983), 249
[9] C. A. Ahravci and M. O. Pekguleryuz, Calphad 22 (1998), 147–155
[10] R. M. K. Young and T. W. Clyne, Script. Metall. 15 (1981), 1211–1216
[11] A. Griger and V. Stefaniay, J. Mat. Sci. 31 (1996), 6645–6652